

Fluoride as a Probe for H-Bonding Interactions in the Active Site of Heme Proteins: The Case of *Thermobifida fusca* Hemoglobin

Francesco P. Nicoletti,^{†,‡} Enrica Droghetti,^{†,‡} Leonardo Boechi,[‡] Alessandra Bonamore,[§] Natascia Sciamanna,[§] Darío A. Estrin,[‡] Alessandro Feis,[†] Alberto Boffi,[§] and Giulietta Smulevich^{*,†}

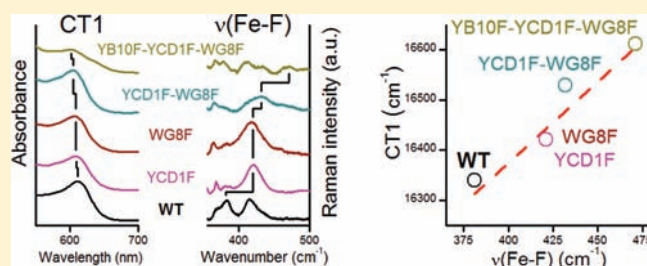
[†]Dipartimento di Chimica “Ugo Schiff”, Università di Firenze, Via della Lastruccia 3-13, I-50019 Sesto Fiorentino (FI), Italy

[‡]Departamento de Química Inorgánica, Analítica y Química Física/INQUIMAE-CONICET, Facultad de Ciencias Exactas y Naturales, Universidad de Buenos Aires, Ciudad Universitaria, Pabellón II, Buenos Aires (C1428EHA), Argentina

[§]Institute Pasteur, Fondazione Cenci Bolognetti, Department of Biochemical Sciences and CNR, Institute of Molecular Biology and Pathology, University of Rome “La Sapienza”, Piazzale Aldo Moro 5, I-00185 Rome, Italy

S Supporting Information

ABSTRACT: The structural and functional properties of the active site of the bacterial hemoglobin from *Thermobifida fusca* are largely determined by three polar amino acids: TrpG8, TyrCD1, and TyrB10. We have exploited the availability of a combinatorial set of mutants, in each of which these three amino acids have been singly, doubly, or triply replaced by a Phe residue, to perform a detailed study on H-bonding interactions between the protein and heme-bound fluoride. By appropriate choice of the excitation conditions, $\nu(\text{Fe}-\text{F})$ stretching bands have been detected in the resonance Raman spectra. In the wild-type protein and one of the mutants, two $\nu(\text{Fe}-\text{F})$ bands have been observed and assigned to the presence of two protein conformers where fluoride is singly or doubly H-bonded. Furthermore, by plotting the CT1 charge-transfer transition energy vs the $\nu(\text{Fe}-\text{F})$ wavenumbers, an empirical correlation has been found. The data are well fitted by a straight line with a positive slope. The position along the correlation line can be considered as a novel, general spectroscopic indicator of the extent of H-bonding in the active site of heme proteins. In agreement with the spectroscopic results, we have observed that the rate of ligand dissociation in stopped-flow kinetic measurements progressively increases upon substitution of the H-bonding amino acids. Molecular dynamics simulations have been performed on the fluoride complexes of native and mutated forms, indicating the prevalent interactions at the active site. All the techniques yield evidence that TrpG8 and TyrCD1 can form strong H bonds with fluoride, whereas TyrB10 plays only a minor role in the stabilization of the ligand.



INTRODUCTION

One of the key objectives of current research in heme proteins is to find well-defined correlations between functional aspects and chemical properties of the active site. There are three main determinants for the reactivity of the active site of heme proteins, namely, oxidation and spin state of the iron ion, “proximal” iron coordination to the protein matrix, and “distal” cavity environment. The latter is essentially defined by the protein amino acids which can stabilize (or destabilize) the iron-bound ligands through a manifold of interactions. H-bonding often appears to play a significant role in determining the degree of ligand stabilization, in the form of single residue-to-ligand H-bonds,^{1,2} water-mediated H-bonds,³ or even ligand inclusive H-bond networks.^{4–7} Therefore, experimental methods which can selectively and sensitively probe H-bonding interactions are highly valuable.

Optical spectroscopic methods have been employed in research on heme protein chemistry both with physiological and nonphysiological ligands. Advanced technique⁸ and site-directed

mutagenesis⁹ were extensively applied to globins in general, and myoglobin in particular, thus contributing to create the concept of “myoglobin as a molecular laboratory”.¹⁰ More recently, however, the discovery of novel natural variations on the globin theme has provided new impetus on heme protein research. In particular, a large family of globins of bacterial origin characterized by a two-over-two helical structure (instead of the typical three-over-three), and by a remarkable variability in the nature of the amino acid residues within the heme active site, have been identified as truncated hemoglobins (trHbs).¹¹ The trHb from the actinomyces *Thermobifida fusca* (Tf-trHb)¹² exemplifies the structural properties of this subfamily of proteins. Its polar distal residues, TrpG8, TyrCD1, and TyrB10, provide three potential H-bond donors to stabilize the incoming ligands. The role of these residues has been recently addressed in a combinatorial set of mutants in which each amino acid has been replaced singly by a

Received: October 3, 2011

Published: November 17, 2011

Phe residue, and also by preparation of double and triple mutants. This unique collection of mutants, in which the highly polar distal environment is progressively transformed in a fully hydrophobic cavity, has been investigated by functional and spectroscopic studies that clearly indicated that TrpG8 and TyrCD1 are the residues mainly involved in the stabilization of exogenous ligands, namely sulfide in the Fe(III) state¹³ and CO in the Fe(II) state.¹⁴

In the present work, we exploit the high sensitivity of fluoride complexes to probe H-bonding in the distal cavity of Tf-trHb. Our results rest on a very recent rediscovery of the potential of combined resonance Raman (RR) and electronic absorption spectroscopy of fluoride-bound heme proteins.¹⁵ We have now tested this method on the benchmark of the combinatorial set of Tf-trHb mutants. The spectroscopic results for the eight proteins are compared with kinetic and computational results, showing a good agreement. The analysis of the results leads to a novel correlation between the $\nu(\text{Fe}-\text{F})$ vibrational frequency and the CT1 transition energy.

EXPERIMENTAL SECTION

Abbreviations. trHb, truncated hemoglobin; Tf, *Thermobifida fusca*; ASV, acidic surface variant of Tf containing two single site mutations Phe107Glu and Arg91Glu; DHP, dehaloperoxidase; HRPc, horseradish peroxidase isoenzyme C; hhMb, horse heart myoglobin; swMb, sperm whale myoglobin; MES, 2-(*N*-morpholino)ethanesulfonic acid; TRIS, tris(hydroxymethyl)aminomethane; MD, molecular dynamics; RR, resonance Raman; 6c, six-coordinate; HS, high spin; CT, charge transfer; WT, wild type.

Genetic Engineering Procedures. Wild type (WT) Tf-trHb was expressed as a recombinant protein in *Escherichia coli* cells and purified as described previously.¹² As previously reported,¹⁴ the acidic surface variant (ASV) of Tf-trHb differs from the WT protein by mutation of both Phe107 and Arg91 to glutamic acid to increase protein solubility during recombinant expression, without affecting thermostability or ligand binding properties. Therefore, ASV was taken as an engineered scaffold of the WT protein for subsequent site-directed mutagenesis studies on the relevant residues of the distal heme pocket. In particular, our study included the single, double, and triple mutants in which the polar distal amino acids [TyrB10(54), TyrCD1-(67), and TrpG8(119)] were replaced with Phe residues. Seven distal mutants of ASV were studied, namely, TrpG8→Phe (hereafter WG8F), TyrCD1→Phe (YCD1F), TyrB10→Phe (YB10F), TyrB10→Phe-TrpG8→Phe (YB10F-WG8F), TyrCD1→Phe-TrpG8→Phe (YCD1F-WG8F), TyrB10→Phe-TyrCD1→Phe (YB10F-YCD1F), and TyrB10→Phe-TyrCD1→Phe-TrpG8→Phe (YB10F-YCD1F-WG8F).

Sample Preparation. All measurements were performed at room temperature. Fluoride and phosphate salts were obtained from Merck AG (Darmstadt, Germany), and Sephadex G-25 from Pharmacia Biotech (Uppsala, Sweden). 2-[*N*-Morpholino]ethanesulfonic acid (MES) and tris(hydroxymethyl)aminomethane (TRIS) were bought from Sigma-Aldrich (Steinheim, Germany). All chemicals were of analytical or reagent grade and were used without further purification. The fluoride complexes were prepared by adding a 0.5 M buffered solution of NaF to the Fe(III) proteins, giving a final concentration of 0.2 M. Buffers (0.1 M) were used for experiments at pH 8.5 (TRIS), 7.0 (phosphate), 5.5 (MES). The sample concentration was in the range of 50–100 μM . The fluoride complexes of the YB10F-WG8F, YCD1F-WG8F, YB10F-YCD1F, YB10F-YCD1F-WG8F Tf-trHb mutants were obtained after the oxidation of the Fe(II) form (present in a mixture with the Fe(III) form) using excess potassium ferricyanide followed by gel filtration on a Sephadex G-25 column to remove the oxidant.

Spectroscopic Characterization. Electronic absorption spectra, measured with a double-beam spectrophotometer (Varian Cary 5), were recorded using a 1 cm cuvette and a 600 nm/min scan rate. Absorption spectra (using a 5-mm NMR tube) were measured both prior to and after RR measurements, ensuring that no degradation had taken place under the experimental conditions used. RR spectra were measured with excitation at 406.7 nm (Kr⁺ laser, Coherent, Innova 300C) and 441.6 nm (He–Cd laser, Kimmon IK4121R-G) using a triple spectrometer (consisting of two Acton Research SpectraPro 2300i working in the subtractive mode, and a SpectraPro 2500i in the final stage with a 3600 grooves per millimeter grating), equipped with a liquid-nitrogen cooled CCD detector (Roper Scientific Princeton Instruments). RR spectra were calibrated with indene, *n*-pentane, and carbon tetrachloride as standards to an accuracy of 1 cm^{-1} for intense isolated bands.

All RR measurements were repeated several times under the same conditions to ensure reproducibility. To improve the signal-to-noise ratio, a number of spectra were accumulated and summed only if no spectral differences were noted. To determine peak bandwidth and positions, a curve-fitting program (Lab Calc; Galactic) was used to simulate the spectra using a mix of (50%) Gaussian and (50%) Lorentzian line shapes. Bandwidths (full width at half-maximum) varied as follows: 9–12 cm^{-1} for the $\delta(\text{C}_\beta\text{C}_\alpha\text{C}_\alpha)$ propionyl modes, 11–12 cm^{-1} for the $\delta(\text{C}_\beta\text{C}_\alpha\text{C}_\beta)$ vinyl modes, 13–20 cm^{-1} for the $\nu(\text{Fe}-\text{F})$ stretching mode.

Kinetic Measurements. Ligand binding and release were carried out by stopped flow measurements using an Applied Photophysics apparatus (Leatherhead, UK). Fluoride and azide binding kinetics were measured by mixing Fe(III) WT or mutated proteins with increasing concentrations of NaF or NaN₃ solutions in 50 mM phosphate buffer at pH 7.0. Protein concentrations were in the range 4–8 μM , and observation wavelengths were 404 nm for fluoride and 414 nm for azide. Fluoride release kinetics were measured according to the ligand displacement methods by mixing fluoride-bound proteins with 0.1 M NaN₃ solutions in 50 mM phosphate buffer at pH 7.0 and monitoring the absorbance decrease at 404 nm. Under these experimental conditions, given the higher affinity and faster binding kinetics of N³⁻ with respect to fluoride, the observed signal decay reflected uniquely the contribution from the fluoride release process. Ligand binding data were fitted to standard second-order equations, and ligand release to mono-exponential decays by using the Matlab program (South Natick, MA).

Molecular Dynamics Simulations. The simulations were performed starting from the crystal structure of WT Tf-trHb, solved at 2.48 Å resolution (PDB entry: 2BMM.pdb). The fluoride was added in the distal site, bound to Fe with a bond distance of 1.8 Å. Each simulation was performed using WT and ASV proteins, single mutant (YB10F, WG8F), double mutant (YCD1F-WG8F), and triple mutant proteins (YB10F-YCD1F-WG8F). The system was then immersed in a box of TIP3P water molecules.¹⁶ The minimum distance between protein and wall was 10 Å, and all systems were simulated employing periodic boundary conditions and Ewald sums for treating long-range electrostatic interactions.¹⁷ The shake algorithm was used to keep bonds involving H atoms at their equilibrium length. This allowed us to employ a 2 fs time step for the integration of Newton's equations. The parm99 set of parameters implemented in AMBER was used to describe the protein.¹⁸ The charges and parameters for Fe(III) heme–fluoride were determined by the standard procedure: partial charges were computed using the restricted electrostatic potential (RESP) recipe and DFT electronic structure calculations with the PBE functional and 6-31G** basis sets (Table S1, Supporting Information). The calculation has been performed in the high spin state, which is known to be the ground state. Equilibrium distance and angles, as well as force constants, were computed using the same methods and basis set used for computed charges. The Lennard–Jones parameters of the coordinated fluoride were taken from parm99 parameters. The temperature and pressure were regulated with the Berendsen thermostat and barostat, respectively, as

implemented in AMBER. All systems were minimized to optimize any possible structural clashes. Subsequently, the systems were heated slowly from 0 K to 300 K using a time step of 0.1 fs, under constant volume conditions. Finally, a short simulation at constant temperature of 300 K, under constant pressure of 1 bar, was performed using a time step of 0.1 fs, to allow the systems to reach proper density. These equilibrated structures were the starting point for 30 ns of MD simulations. All systems were stable during the time scale of the simulations as shown by the inspection of the root-mean-square displacements (rmsd) depicted in Figure S1, Supporting Information.

RESULTS

Spectroscopy. We first investigated the electronic absorption and RR spectra (recorded with both 406.7 and 441.6 nm excitation wavelengths) of the fluoride complexes of WT and ASV Tf-trHb, and of the combinatorial set of the distal mutants. The UV–visible absorption spectra (Figure 1) displayed Soret bands at 406–403 nm and Q bands at 485–491 nm. These features, and the high-frequency RR spectra obtained with 441.6 nm excitation (data not shown), are characteristic of six-coordinate (6c) HS forms, with fluoride coordinated as the sixth ligand of the iron ion. In the low frequency RR spectra, the $\nu(\text{Fe–F})$ stretching mode was assigned on the basis of its intensity enhancement upon excitation near the CT2 band, as shown by the comparison of the RR spectra obtained with excitation 406.7 and 441.6 nm (Figure 1, right).¹⁵ The spectra of the various proteins differed in the wavelength of the CT1 band and the wavenumber of the $\nu(\text{Fe–F})$ stretching mode, indicating a different interaction between the bound fluoride and the distal polar residues. WT and ASV were characterized by almost identical spectra with a CT1 maximum at 612 nm and the $\nu(\text{Fe–F})$ stretch at 381 cm^{-1} , overlapping a propionyl bending mode. The low energy of the CT1 band, together with the low frequency of the $\nu(\text{Fe–F})$ stretch, indicates the presence of strong H-bonding interactions between fluoride and the distal cavity residues, consistent with the presence of multiple H-bonds donated to the fluoride by the distal residues.¹⁵ In addition, we assigned a band at 420 cm^{-1} to a second $\nu(\text{Fe–F})$ stretching mode on the basis of both CT2 excitation enhancement (Figure 1, right) and correlation with the $\nu(\text{Fe–F})$ frequencies of the set of mutants (see below). This band indicates the presence of a second complex with a weakly H-bonded fluoride. The frequencies of the two $\nu(\text{Fe–F})$ bands are identical for both WT and ASV, and their relative intensities are very similar, as shown by a band-fitting analysis (Figure 2).

Distal mutations affected the spectral position of both the CT1 and $\nu(\text{Fe–F})$ stretch to different extents. Among the singly mutated variants, minor changes were observed upon mutation of TyrB10 to Phe: an upshift by 1 nm of the CT1 band and an increase of the $\nu(\text{Fe–F})$ band at 381 cm^{-1} at the expense of the one at 421 cm^{-1} (Figures 1 and 2). On the other hand, the spectra of the YCD1F and WG8F mutants gave rise to spectra which were similar to each other but different from those of WT and ASV. The CT1 band shifted to 609 nm, and a single $\nu(\text{Fe–F})$ band at 421 cm^{-1} was observed. In regard to the doubly mutated variants, YB10F-YCD1F, in which both distal Tyr residues are missing, and YB10F-WG8F, in which TyrB10 and TrpG8 are mutated, gave rise to similar results. The YB10F-WG8F variant had a CT1 at 610 nm and the $\nu(\text{Fe–F})$ band at 415 cm^{-1} , while the YB10F-YCD1F variant had a CT1 at 609 nm and the $\nu(\text{Fe–F})$ band at 419 cm^{-1} . However, in the

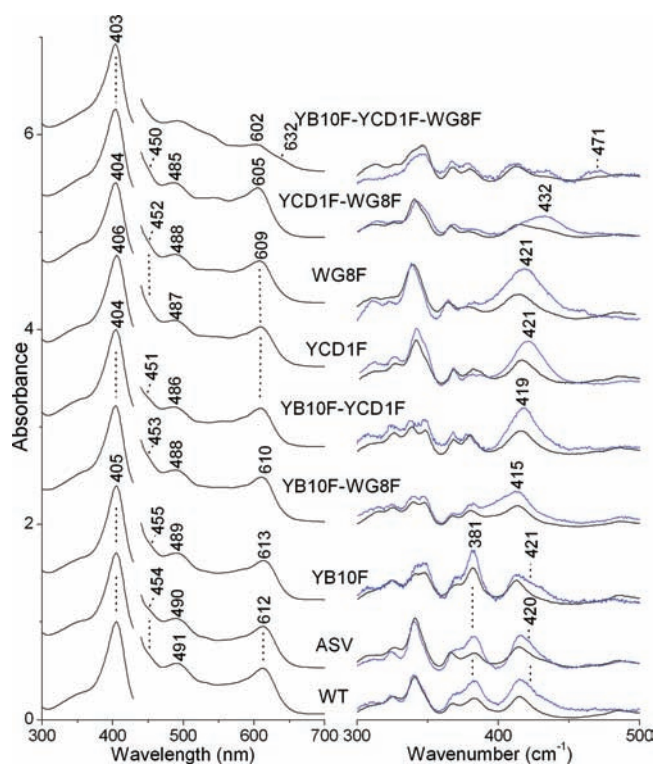
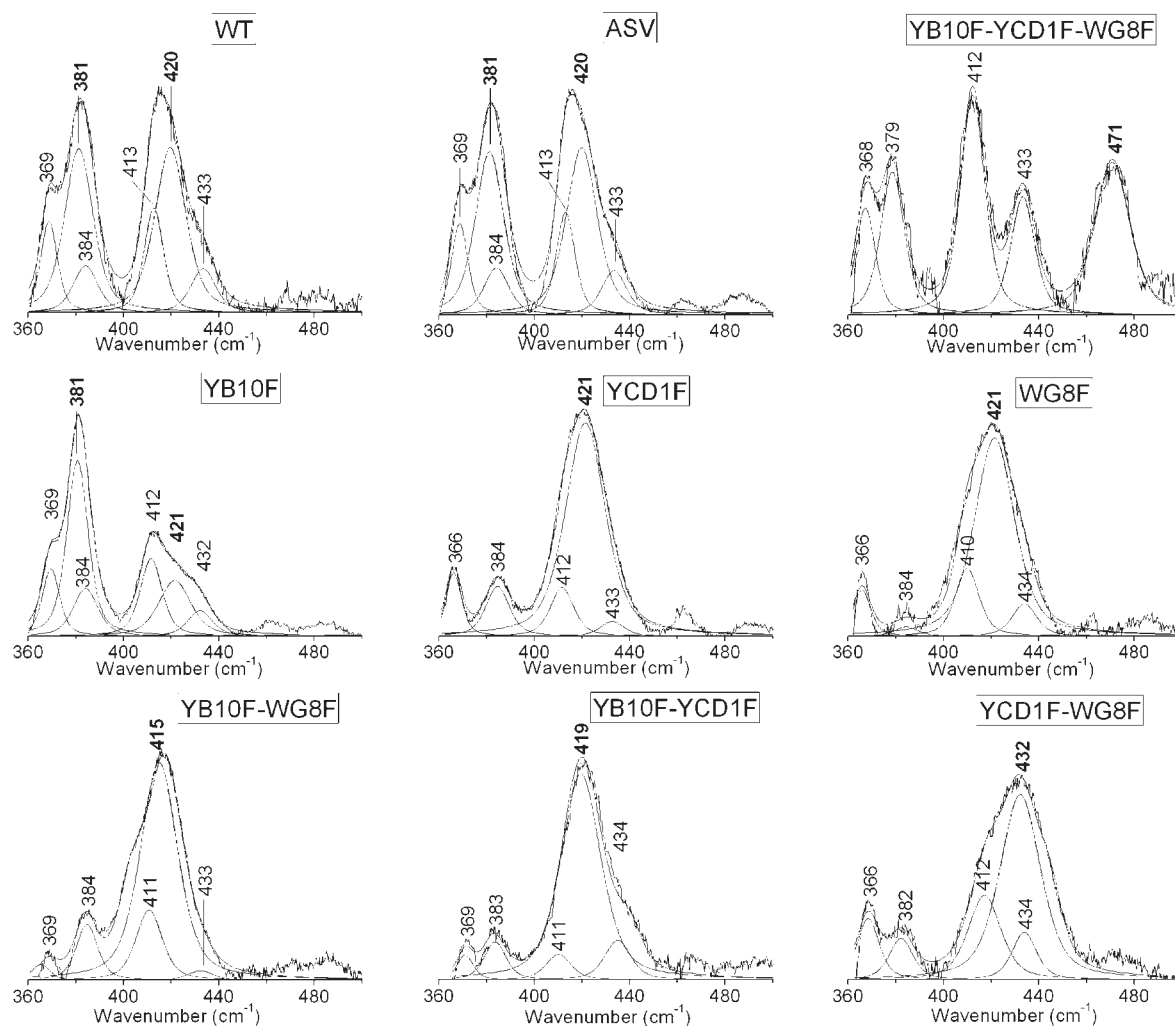


Figure 1. UV-vis (left) and resonance Raman (right) spectra of the fluoride complexes of Tf-trHb WT, ASV and the distal variants at pH 7.0 (0.1 M phosphate). Left: the region between 440 nm and 700 nm has been expanded five-fold. Spectra have been shifted along the ordinate axis to allow better visualization. Right: the RR spectra were taken with excitation in resonance with the Soret (406.7 nm, black line) and with the CT2 band (441.6 nm, blue line). Experimental conditions: 1 cm^{-1} spectral resolution; 406.7 nm: 10 mW laser power at the sample, average of ten spectra with 1800 s integration time (WT and ASV), average of eight spectra with 1800 s integration time (YB10F), average of six spectra with 600 s integration time (YB10F-WG8F), average of six spectra with 650 s integration time (YB10F-YCD1F), average of five spectra with 900 s integration time (YCD1F), average of ten spectra with 700 s integration time (WG8F), average of five spectra with 900 s integration time (YCD1F-WG8F), average of twelve spectra with 400 s integration time (YB10F-YCD1F-WG8F); 441.6 nm: 25 mW laser power at the sample, average of six spectra with 1800 s integration time (WT and ASV), average of six spectra with 1200 s integration time (YB10F), average of ten spectra with 800 s integration time (YB10F-WG8F), average of ten spectra with 750 s integration time (YB10F-YCD1F), average of nine spectra with 1000 s integration time (YCD1F), average of twelve spectra with 900 s integration time (WG8F), average of ten spectra with 800 s integration time (YCD1F-WG8F), average of twenty-five spectra with 400 s integration time (YB10F-YCD1F-WG8F). A baseline has been subtracted from all spectra.

YCD1F-WG8F mutant, where both the TyrCD1 and TrpG8 are replaced by Phe, the CT1 band further blue-shifted to 605 nm and the $\nu(\text{Fe–F})$ band moves up to 432 cm^{-1} . These values suggest the presence of a weak interaction between the TyrB10 and the bound fluoride. Finally, the YB10F-YCD1F-WG8F triply mutated variant was not fully bound with fluoride at 0.2 M concentration, being a mixture of two 6cHS forms, an aquo 6cHS heme (CT1 at 632 nm) and a 6cHS fluoride complex. This latter form showed a CT1 band at 602 nm and a Raman band at 471 cm^{-1} which, being enhanced upon 441.6 nm excitation, is assigned to the $\nu(\text{Fe–F})$ stretch.



Protein	$\delta(C_{\beta}C_cC_d)$		$\delta(C_{\beta}C_aC_b)$		$\nu(\text{Fe-F})$	
YB10F-YCD1F-WG8F	368 (9)	379 (12)	412 (11)	433 (12)	471 (18)	
YCD1F-WG8F	366 (9)	382 (12)	412 (11)	434 (12)	432 (20)	
WG8F	366 (9)	384 (12)	410 (11)	434 (12)	421 (20)	
YCD1F	366 (9)	384 (12)	412 (11)	433 (12)	421 (20)	
YB10F-YCD1F	371 (9)	383 (12)	411 (11)	434 (12)	419 (20)	
YB10F-WG8F	369 (9)	384 (12)	411 (11)	433 (12)	415 (18)	
YB10F	369 (9)	384 (12)	412 (11)	432 (12)	421 (16)	381 (13)
ASV	369 (9)	384 (12)	413 (11)	433 (12)	420 (16)	381 (15)
WT	369 (9)	384 (12)	413 (11)	433 (12)	420 (16)	381 (15)

Figure 2. RR spectra in the 360–490 cm^{-1} region with the corresponding band-fitting analysis. Experimental conditions: see Figure 1. The $\nu(\text{Fe-F})$ bands are indicated in bold. The table reports the assignment of the bands with their frequency and bandwidth (in brackets) as obtained by the band-fitting analysis.

Table 1 reports the CT1 band maxima together with the frequencies of the $\nu(\text{Fe-F})$ and the $\nu(\text{C=C})$ stretching modes (see below) for the proteins under investigation. The data for sperm whale myoglobin (swMb), horse heart myoglobin (hhMb), dehaloperoxidase (DHP), and horseradish peroxidase isoenzyme C (HRPC) are also included for comparison.

Fluoride Binding and Release Kinetics. Ligand binding kinetics, measured in stopped flow experiments, revealed slight differences in the second-order binding rates among the different

mutated proteins. As reported in Table 2, fluoride binding proceeded at rates between 4 and 8 $\text{mM}^{-1} \text{s}^{-1}$, whereas azide binding rates were about 80-fold higher. In turn, 200-fold differences were observed in the rates of fluoride release among the different mutants, the WT protein being the slowest (1.2 s^{-1}) and YB10F-YCD1F-WG8F being the fastest (242 s^{-1}). Azide dissociation constants could not be measured directly and were calculated from the ratio between the second-order ligand binding rates and the measured thermodynamic constants

Table 1. CT1 Band Maxima (expressed in nm and cm^{-1}) Together with the Wavenumbers of the $\nu(\text{Fe}-\text{F})$ and the Vinyl Group $\nu(\text{C}=\text{C})$ Stretching Modes for the Proteins under Investigation^a

protein	CT1 (nm)	CT1 (cm^{-1})	$\nu(\text{Fe}-\text{F})^b$ (cm^{-1})	$\nu(\text{C}=\text{C})$ (cm^{-1})
YB10F-YCD1F-WG8F	602	16611	471	1626
DHP ^d	605	16529	462	1620s, 1632w
YCD1F-WG8F	605	16529	432	1626
hhMb (pH 7.0) ^c	607	16475	460	1620
swMb (pH 7.0) ^c	607	16475	462	1620
WG8F	609	16420	421	1627
YCD1F	609	16420	421	1627
YB10F-YCD1F	609	16420	419	1628
hhMb (pH 5.2) ^c	609	16420	411	1620
swMb (pH 5.2) ^c	609	16420	410	1620
YB10F-WG8F	610	16393	415	1626
HRPC ^c	611	16367	385	1621w, 1631s
WT	612	16340	420 (54%); 381 (46%)	1628
ASV	612	16340	420 (53%); 381 (47%)	1628
YB10F	613	16313	421 (32%); 381 (68%)	1627

^aThe data for sperm whale myoglobin (swMb), horse heart myoglobin (hhMb), dehaloperoxidase (DHP), and horseradish peroxidase isoenzyme C (HRPC) are also included for comparison. ^bThe relative percentage of the two $\nu(\text{Fe}-\text{F})$ conformers, as found by the curve-fitting analysis, is reported in brackets. ^cReferences 15 and 32. ^dReference 39.

Table 2. Fluoride Binding and Dissociation Kinetics for Tf-trHb and Its Distal Side Mutants^a

protein	$k_{\text{on}}(\text{F}^-)$, $\text{mM}^{-1} \text{s}^{-1}$	$k_{\text{off}}(\text{F}^-)$, s^{-1}
ASV	6.4 ± 0.6	1.2 ± 0.08
WT	6.5 ± 0.4	1.7 ± 0.07
YB10F	5.5 ± 0.3	29 ± 0.11
YCD1F	4.2 ± 0.6	9 ± 0.12
WG8F	4.5 ± 0.5	30.2 ± 0.26
YB10F-YCD1F	6.0 ± 0.5	49 ± 0.09
YB10F-WG8F	5.4 ± 0.3	106 ± 0.35
YCD1F-WG8F	6.6 ± 0.4	117 ± 1.25
YB10F-YCD1F-WG8F	7.6 ± 0.4	242 ± 12.75

^aAll experiments were carried out in 50 mM phosphate buffer at pH 7.0 at 25 °C. Ligand dissociation rates were obtained by fluoride displacement with 0.1 M sodium azide.

(see Table S2, Supporting Information). Azide release rates were found to follow the same trend as the fluoride release rates, although the overall effect of the mutations was slightly damped with respect to fluoride.

Computer Simulations. To obtain the charge distribution of the active site, we performed DFT electronic structure calculations using the PBE functional and the 6-31G** basis set of a model system composed of fluoride coordinated to an isolated Fe(III) heme with imidazole as the sixth ligand. The calculations were performed on the HS state as identified by the spectroscopic measurements. In agreement with the experimental results, the optimized Fe–F bond distance was found to be ~ 1.8 Å and the coordinated fluoride exhibited a negative charge (partial charge of $-0.36 e^-$), highlighting that positive residues should stabilize the coordinated fluoride, similar to the results found for the heme-bound O_2 .^{19–22}

Classical molecular dynamics (MD) simulations of Fe(III) Tf-trHb with coordinated fluoride were then performed to shed light on the nature of the H-bond network stabilizing the

coordinated fluoride, as suggested by the spectroscopy data. No significant structural differences were found in the active site environment during the time scale of the simulation between WT and ASV (Figure 3A and S2), confirming that Phe107 and Arg91 mutations do not affect the ligand binding properties. Moreover, in both the WT and ASV proteins, the coordinated fluoride is stabilized by a H-bond with the indole N proton of the WG8 and the hydroxylic hydrogen of the YCD1, while the TyrB10 residue is not involved (Figure 3A). The same result was found for the YB10F mutant (Figure 3B), indicating that the YB10 residue has a minor role in the stabilization of the coordinated fluoride. Accordingly, when TrpG8 is replaced by Phe, the YCD1 residue mainly stabilizes the coordinated fluoride, while the YB10 is not able to form a strong H-bond with the ligand (Figure 3C). However, the hydroxylic hydrogen of the YB10 residue is able to interact with the coordinated fluoride when both WG8 and YCD1 are absent, as revealed for the YCD1F-WG8F double mutant (Figure 3D).

The triple mutant YB10F-YCD1F-WG8F was able to accommodate two water molecules in the active site (Figure 4, upper panel). To characterize the internal water interactions, we evaluated the radial distribution function $g(r)$ for the O atom of water molecules, centered in the coordinated fluoride for the last 25 ns of the simulation. The integration of the $g(r)$ function confirmed the presence of two water molecules around the F^- anion (Figure 4, lower panel). The profiles shows a clear peak at 2.75 Å, indicating the presence of water molecules interacting strongly with the coordinated fluoride.

DISCUSSION

Distal Cavity Interactions. Fluoride is a common ligand for heme proteins in the Fe(III) state. It is not known as a physiological ligand, and only recently has it been reported that it can modulate the reactivity of a heme protein.²³ Nevertheless, fluoride complexes of heme proteins as model systems have been actively researched with optical and magnetic methods during

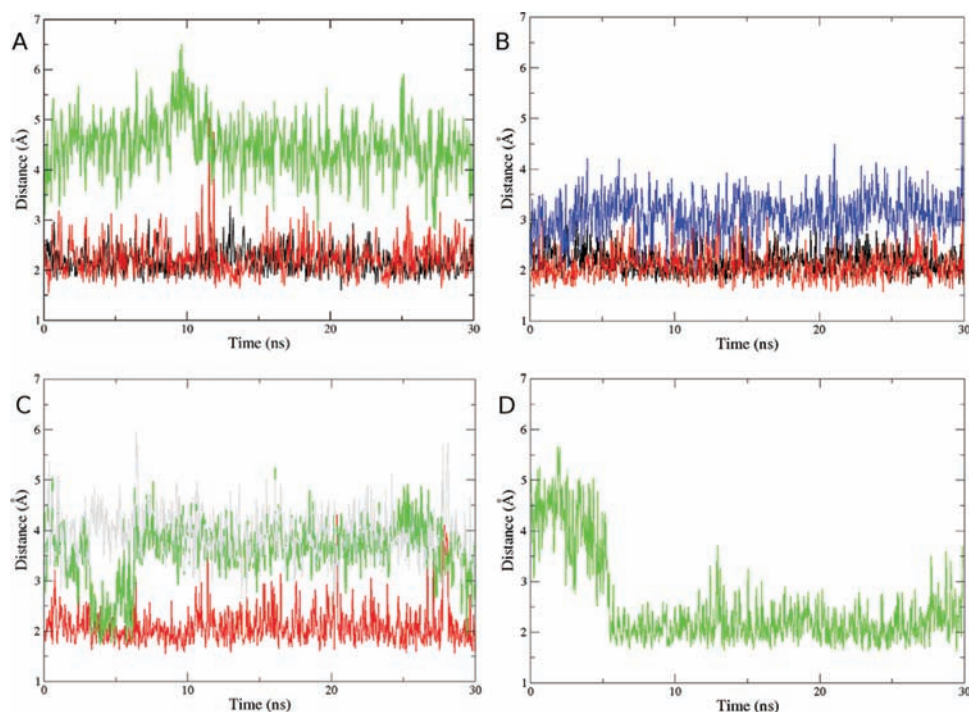


Figure 3. Time evolution of selected distances of Tf-trHb. (A) WT protein; (B) YB10F mutant; (C) WG8F mutant; (D) YCD1F-WG8F mutant. (Black) Distances between fluoride and indole N proton of the WG8; (red) distances between fluoride and hydroxylic hydrogen of the YCD1; (green) distances between fluoride and hydroxylic hydrogen of the YB10; (blue) distances between indole N proton of the WG8 and the hydroxylic oxygen of the YCD1; (gray) distances between hydroxylic hydrogen of the YCD1 and the hydroxylic oxygen of the YB10.

recent decades. Fluoride is a weak-field ligand; therefore, it binds heme proteins, giving rise to 6CHS complexes, characterized by a strong Soret band with maxima between 404 and 406 nm and a weaker Q-band at 490 nm.^{24–27} In addition, ligand-to-metal charge transfer transitions between 607 and 617 nm [CT1 due to $a_{2u}(\pi) \rightarrow e_g(d_{\pi})$ transition, with x,y polarization] and between 450 and 460 nm [CT2 due to $a'_{2u}(\pi) \rightarrow a_{1g}(d_{z^2})$ with z -polarization] are observed.²⁸ The $\nu(\text{Fe}-\text{F})$ stretching mode is intensified in the Raman spectra obtained in resonance with either the CT1 or the CT2 band.^{15,24,29–31} Fluoride builds four sp^3 hybrid orbitals and coordinates to the heme iron via σ - and π -bonding. An (lone pair) sp^3 hybrid orbital forms a σ bond with the d_{z^2} Fe orbital. In this case the d_{π} metal orbitals (d_{xz} , d_{yz} , d_{xy}) do not interact with the ligand orbitals and remain as nonbonding orbitals centered on the metal. Fluoride is also capable of π -bonding, acting as a π -donor. In this case the occupied ligand orbitals are lower in energy than the d_{π} metal orbitals which become π^* and are shifted to higher energy.

We have recently shown¹⁵ that the spectroscopic properties of the fluoride complexes provide a simple and direct method to monitor the interactions of the distal heme pocket environment with the iron-bound ligand. In particular, we have demonstrated a strong correlation between the wavelength of the CT1 band and the strength of H-bonding donation from the distal amino acid side chains to the fluoride ion. In fact, the CT1 maximum wavelength is a sensitive probe of axial ligand polarity and of its interaction with the distal protein residues. It red-shifts when the π -donor capability of the axial ligands decreases, or when the ligand acts as a H-bond acceptor, because the destabilizing interaction between the π orbitals of the ligand and the iron d_{π} orbitals is reduced in these cases.³² In parallel, RR spectra with excitation within the CT2 band (450–460 nm) have revealed

that the $\nu(\text{Fe}-\text{F})$ stretching frequency is directly affected by H-bonding to the fluoride ion. This is mainly due to the reduction of the Fe–F bond strength in H-bonded complexes, as a consequence of a decreased electron density on fluoride. A low $\nu(\text{Fe}-\text{F})$ stretching frequency has been shown to correlate with a red-shifted CT1 band in the complexes where fluoride is strongly H-bonded to distal pocket residues. We found that WT and ASV Tf-trHb are characterized by a $\nu(\text{Fe}-\text{F})$ band at 381 cm^{-1} together with a CT1 at 612 nm, similar to the spectroscopic signature of a peroxidase, in agreement with the presence of strong H-bonding residues. The present results show that the distal mutations markedly affect the spectroscopic markers of the fluoride adducts. In particular, because in the absence of either TrpG8 or TyrCD1, the $\nu(\text{Fe}-\text{F})$ band shifts from 381 cm^{-1} to higher frequency, with a concomitant blue-shift of the CT1 band, we clearly demonstrate that the $\nu(\text{Fe}-\text{F})$ band at 381 cm^{-1} together with the CT1 at 612 nm correspond to a conformer where the bound fluoride is stabilized by H-bond interactions donated by both TrpG8 and TyrCD1. Interestingly, in the presence of TrpG8 and TyrCD1, TyrB10 does not interact with the ligand. In contrast, its absence favors a strengthening of the H-bond, as observed in the single YB10F and in the double YB10F-WG8F and YB10-YCD1 mutants. TyrB10 is able to weakly interact with fluoride only when H-bond interactions with both TrpG8 and TyrCD1 are missing, i.e., in the YCD1F-WG8F double mutant. Accordingly, MD simulations revealed that in the WG8F mutant only the TyrCD1 residue stabilizes the coordinated fluoride, and the TyrB10 residue is not able to form a H-bond with the ligand. However, in the double mutant YCD1F-WG8F, the TyrB10 residue is now able to interact with the coordinated fluoride.

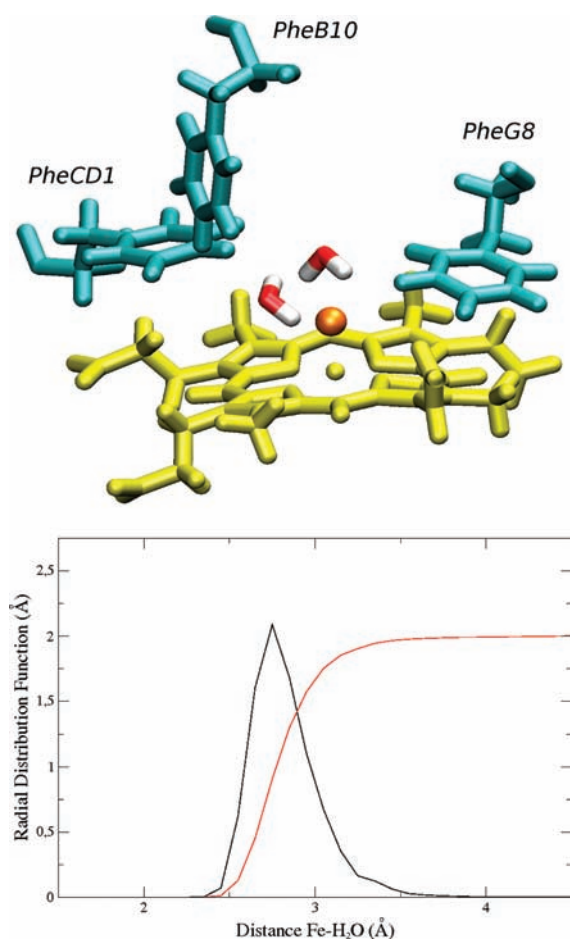


Figure 4. MD simulation obtained for the YB10F-YCD1F-WG8F Tf-trHb triple mutant. Upper panel: Representative snapshot of the active site. Heme group (yellow) with coordinated F^- (orange), relevant residues (cyan), and water molecules inside the active site are depicted. Lower panel: Radial distribution function $g(r)$ plot for the O atom of water molecules, centered in the coordinated fluoride (black). The integrated function, which indicates the total number of water molecules around fluoride, is depicted in red.

A second form of the fluoride complex, which is characterized by a $\nu(\text{Fe}-\text{F})$ band at 420 cm^{-1} , has been found in both the WT and ASV RR spectra. This heterogeneity can be compared with previous results obtained for the fluoride complexes of globins. X-ray diffraction of fluoride-bound hemoglobin indicated an equilibrium between two species, with and without H-bonding between the anion and a water molecule.³³ Accordingly, RR spectra displayed two $\nu(\text{Fe}-\text{F})$ stretches at 443 and 471 cm^{-1} .²⁹ Two pH-dependent forms were found for fluoride-bound myoglobin. The strong band observed at about 460 cm^{-1} at pH 7.0^{15,24,30} decreased in intensity at pH 5.2, with the concomitant growth of a new band at about 410 cm^{-1} .¹⁵ Furthermore, the downshift of the $\nu(\text{Fe}-\text{F})$ stretching mode was accompanied by a 2 nm red shift of the CT2 band (from 607 to 609 nm).^{15,24} These pH-dependent spectral variations were interpreted as due to changes in the iron-fluoride bond distance and/or change in the H-bonds involving the ligand, a water molecule, and the distal His.²⁴ The X-ray structure of the fluoride complex of swMb at pH 7.0 indicated that fluoride is H-bonded to the distal His64 and to a water molecule which, interacting also with the distal His,

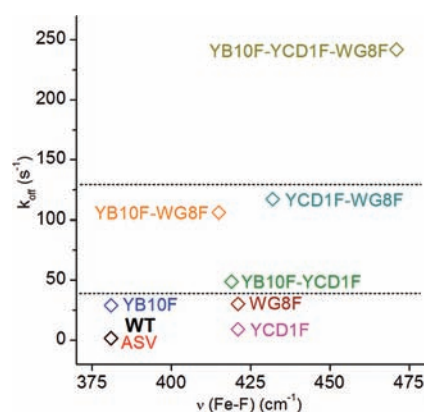


Figure 5. Correlation between the $\nu(\text{Fe}-\text{F})$ wavenumbers (Table 1) and the dissociation kinetics constant (Table 2). The dashed lines separate groupings of triple, double, and single mutants.

stabilizes the coordinated fluoride ion.³⁴ Therefore, protonation of the distal His can occur at acid pH. In the case of WT and ASV Tf-trHb, no spectroscopic changes are observed in the spectra between pH 5.5 and 8.5 (data not shown). We assign the $\nu(\text{Fe}-\text{F})$ band at 420 cm^{-1} to a second conformer, whose bound fluoride is stabilized by a single strong H-bond. Only this form, in fact, is observed in the mutants where either the WG8 or YCD1 residues have been replaced by Phe (Table 1). However, within the time scale of the simulation, only one conformation has been sampled by MD simulations in WT, ASV, and YB10F Tf-trHb, exhibiting stable H-bonds with both WG8 and YCD1. The absence of the second conformation detected in the RR experiments is probably due to limitations of the classical MD approach employed.

An interesting result is provided by the triple mutant that shows a reduced affinity for fluoride. The spectra of the fluoride-bound YB10F-YCD1F-WG8F mutant display the highest energy CT1 band in the Tf-trHb mutant series (i.e., at 603 nm) together with the highest $\nu(\text{Fe}-\text{F})$ stretch at 471 cm^{-1} . Nevertheless, the heme environment, where fluoride is surrounded by three Phe residues, does not appear to be apolar as would be expected. MD simulations clearly indicate that two water molecules interacting with the coordinated fluoride ion are accommodated into the active site. These data resemble closely those of the swMb-F adduct (607 nm and 462 cm^{-1}), whose anionic ligand is H-bonded to the distal His64 (2.74 \AA) and a water molecule (2.71 \AA), deeply buried in the distal side of the heme cavity.³⁴

In general, the Fe-F stretching frequencies and the MD simulations are consistent with the dissociation kinetic rate constants, because the fluoride complexes of the mutants with multiple H-bonding interactions exhibit lower dissociation rate constants. In agreement with the spectroscopic results, the progressive removal of distal H-bonding contributions to the bound fluoride brings about an increase in the observed rate of ligand release. An exponential correlation between the rate of ligand release and the overall fluoride binding energy would be expected if the Fe-F bond is the only determinant of the ligand dissociation process.⁹ Analysis of the data reported in Table 2 and plotted in Figure 5 indicate that there is a clear correspondence between the Fe-F stretching frequencies and the rates of ligand release. The singly, doubly or triply mutated species appear to gather into separate groups within the “stretching frequency/kinetic rate” correlation plot (see Figure 5). It is noteworthy that

Table 3. Comparison between the Spectroscopic Data Obtained for the CO^a and Fluoride^b Complexes of Tf-trHb, hhMb, swMb, DHP, and HRPC Together with the Proposed Distal H-Bond Interactions with the Exogenous Ligand

protein	$\nu(\text{Fe}-\text{CO})$ (cm ⁻¹)	$\nu(\text{CO})$ (cm ⁻¹)	H-bond interaction		$\nu(\text{Fe}-\text{F})$ (cm ⁻¹)	H-bond interaction	
YB10F-YCD1F-WG8F	494	1955	—		471	H ₂ O	
YCD1F-WG8F	488	1967	—				
	498	1952		YB10	432		YB10
WG8F	491	1962	—				
	497	1942		YCD1	421		YCD1
YCD1F	505	1943	WG8		421	WG8	
YB10F-YCD1F	511	1931	WG8		419	WG8	
YB10F-WG8F	493	1966	—				
	511	1936		YCD1	415		YCD1
YB10F	507	1942	WG8		421	WG8	
	522	1926	WG8	YCD1	381	WG8	YCD1
ASV Tf-trHb	509	1938	WG8		420	WG8	
	518	1920	WG8	YCD1	381	WG8	YCD1
WT Tf-trHb	509	1938	WG8		420	WG8	
	518	1920	WG8	YCD1	381	WG8	YCD1
HRPC	516	1933		H42			
	539	1904	R38	H42	385	R38	H ₂ O
swMb pH 7.0	507	1947		H64	462	H64	H ₂ O
hhMb pH 7.0	509	1944		H64	460	H64	H ₂ O
swMb pH5.1	508 ^d			H64			
swMb pH 5.4 ^e					399 ^e 410	H64 ^{+d}	H ₂ O
swMb pH 3.9	491			H64 ⁺			
DHP pH 7.0	500	1950		H55	462	H55	H ₂ O

^a The data of the CO adducts have been taken from the following: Tf-trHb and its mutants;¹⁴ HRPC;³⁸ swMb pH 7.0;⁴¹ hhMb pH 7.0;⁴⁰ swMb pH 5.1 and pH 3.9;⁴⁷ DHP.³⁷ ^b References 15 and 39. ^c Reference 24. ^d It appears that the pK for H64 protonation is higher in the fluoride complex than in the CO complex.

the YB10F mutants (YB10F, YB10F-WG8F, YB10F-YCD1F, and YB10F-YCD1F-WG8F) display a consistent increase in the kinetics of ligand release with respect to the YB10-containing mutants (YCD1F, WG8F, YCD1F-WG8F), indicating that this residue, though not prominently involved in fluoride ligand hydrogen bonding, is still capable of influencing the ligand release process.

The effects on the dissociation kinetics upon distal mutation maybe more complex than the effects on the Fe–F stretching vibrational frequency. In fact, the latter is related to the H-bonding(s) involving fluoride, whereas the barriers fluoride has to overcome in the whole dissociation pathway will be related to H-bond breaking and, additionally, to the presence of diverse migration paths within the protein matrix. For instance, the fact that dissociation from the single TrpG8→Phe mutant is faster than that from the single TyrCD1→Phe mutant could be interpreted on the basis of the hindrance of the Trp side chain. A detailed interpretation, though, would be speculative at the present stage. Moreover, the presence of two conformers could complicate the picture. In principle, two different rates should be observed, although a single rate is observed if the conformers interconvert rapidly (see, e.g., refs 35 and 36).

Comparison with CO Complexes. Table 3 compares the spectroscopic data for the complexes of Tf-TrHb, hhMb, DHP, and HRPC with CO and fluoride, together with the proposed distal H-bonds involving the ligands.^{14,15,37–41} CO has been shown to be a useful probe of heme-binding sites in Fe(II) proteins, because FeCO back-bonding is modulated by polar interactions with protein residues, and by variations in the donor

strength of the trans ligand.⁴¹ The electrostatic field generated by the polar distal pocket amino acids alters the electron distribution in the FeCO unit, changing the order of the C–O bond. A positively charged electrostatic field favors back-donation, which strengthens the Fe–C bond and correspondingly weakens the C–O bond, thereby increasing the $\nu(\text{FeC})$ vibrational frequency and decreasing the $\nu(\text{CO})$ frequency, readily detectable in infrared and RR spectra. A linear correlation with negative slope between the frequencies of the $\nu(\text{FeC})$ and $\nu(\text{CO})$ stretching modes has been found for a large class of CO complexes of heme proteins, including bacterial trHb's, and heme model compounds containing imidazole as the fifth iron ligand.^{41,44} The $\nu(\text{FeC})/\nu(\text{CO})$ position along the correlation line reflects the type and strength of distal polar interactions.⁴¹

Two conformers were observed in the spectra of the CO complexes of both WT and ASV Tf-trHb: form 1 with $\nu(\text{FeC})$ and $\nu(\text{CO})$ at 509 and 1938 cm⁻¹ and form 2 with $\nu(\text{FeC})$ and $\nu(\text{CO})$ at 518 and 1920 cm⁻¹, respectively. The spectroscopic data and MD simulations demonstrated that CO interacts with TrpG8 in form 1 but with both TrpG8 and TyrCD1 in form 2, while TyrB10 does not directly interact with the bound CO.¹⁴ The present results suggest that the two fluoride conformers in the WT and ASV proteins are stabilized in a similar manner.

When the effects of the mutations are considered, it can be seen that the data obtained from CO complexes and those obtained from fluoride complexes (Table 3) follow a common trend, although the corresponding complexes cannot be placed in the same order. In fact, it is expected that Trp and Tyr mutation to Phe

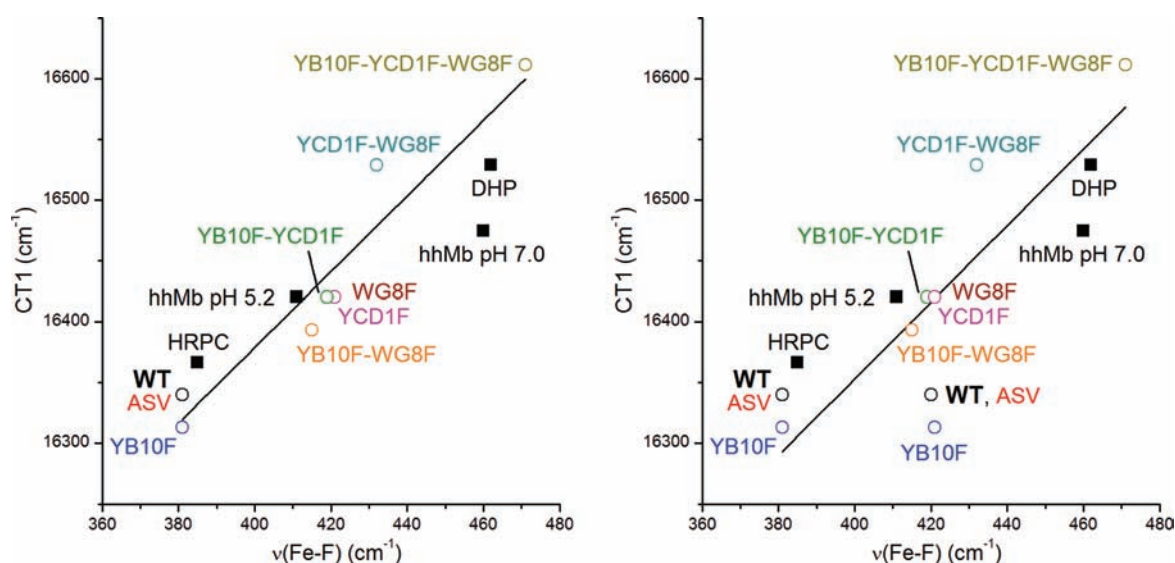


Figure 6. Empirical correlation plot between the $\nu(\text{Fe}-\text{F})$ wavenumbers and the CT1 energy. The frequencies of the CT1 are plotted as a function of the frequencies of the Fe–F stretching modes for the following proteins: WT, ASV, YB10F, YCD1F, WG8F, YB10F-WG8F, YB10F-YCD1F, YCD1F-WG8F, YB10F-YCD1F-WG8F, HRPC, DHP, hhMb pH 7.0, hhMb pH 5.2. Experimental data are reported in Tables 1 and 3. The lines represent two different least-squares fits for the experimental data of WT Tf-trHb and the combinatorial set of mutants, namely, considering only the strongly H-bonded forms of WT, ASV, and YB10F with $\nu(\text{Fe}-\text{F})$ stretch at 381 cm^{-1} (left) and both conformers (right).

decreases both the back-bonding in the CO complexes and the H-bonding interactions in the fluoride complexes. However, the single mutants YCD1F and WG8F, which share very similar CT1 maximum wavelengths and $\nu(\text{Fe}-\text{F})$ stretching frequencies in their fluoride complexes, display very different vibrational frequencies of the FeCO unit. Another divergent mutant is the triple YB10-YCD1-WG8F, which displays the highest $\nu(\text{Fe}-\text{F})$ stretching frequency but an intermediate back-bonding in the CO complex. There are several possible explanations for these differences. Clearly, back-bonding in the CO complexes depends on *all* kinds of polar interactions with the neighboring amino acids,⁴² whereas H-bonding is the only effective stabilization for the heme-bound fluoride. Moreover, it should be considered that the two types of complexes have different chemical properties, namely (i) carbon monoxide is neutral (and almost apolar), whereas fluoride retains a negative charge, and (ii) H-bonding to CO is directional, whereas there is no directionality in F–HX bonding because of the spherical symmetry of fluoride.

CT1 Energy/ $\nu(\text{Fe}-\text{F})$ Wavenumber Correlation. In an attempt to find an empirical correlation between the $\nu(\text{Fe}-\text{F})$ wavenumbers and the CT1 transition energy, we have plotted our experimental data for all the Tf-trHb fluoride complexes together with the available literature data (Figure 6, left). The data are fitted well by a straight line with positive slope. The (CT1)/ $\nu(\text{Fe}-\text{F})$ position along the correlation line appears to reflect the extent of distal H-bonding interactions. Fluoride complexes which are stabilized by multiple, strong H-bond interactions, like those of the WT, ASV Tf-trHb, and YB10F conformer ($\nu(\text{Fe}-\text{F})$ at 381 cm^{-1}), are located at the extreme left side. In fact, H-bonding decreases both the $\nu(\text{Fe}-\text{F})$ stretching frequency and the energy of the $e_g(d_{\pi})$ orbitals, thereby lowering the energy of the $a_{2u}(\pi) \rightarrow e_g(d_{\pi})$ CT1 transition. At the other extreme of the line, fluoride complexes with very weak H-bond interactions are found, like that of the YB10F-YCD1F-WG8F mutant. Unlike the points for the 381 cm^{-1} conformer, those for the second conformer of WT, ASV Tf-trHb,

and YB10F ($\nu(\text{Fe}-\text{F})$ at $420\text{--}421\text{ cm}^{-1}$) fall off the line (Figure 6, right). In fact, the presence of two conformers should give rise to two CT1 absorption bands. Based on the CT1 energy measured for WG8F, YCD1F, and YCD1F-YB10F mutants which show only the second conformer, the expected energy difference between the two conformers is about 200 cm^{-1} . Because the CT1 band is relatively weak and broad, in practice we observe a single maximum. Therefore, given the impossibility to single out two different CT1 bands for WT, ASV, and YB10F, we correlate the two different Raman Fe–F stretches with the same energy value. As a consequence for the proteins with multiple conformers, some points are off the line.

Some deviations from this linear correlation can be expected as a consequence of different vinyl/heme conjugation. In general, the absorption maxima of the heme prosthetic group, including the Soret, Q, and CT1 bands, are related not only to the coordination/spin state of the heme but also to the degree of conjugation between the heme group and its two vinyl substituents, which can cause up to 10 nm red-shift of the electronic transitions.⁴³ In heme proteins, the vinyl groups are found to give rise to $\nu(\text{C}=\text{C})$ polarized Raman bands between 1620 and 1635 cm^{-1} .⁴⁴ A direct relationship between the $\nu(\text{C}=\text{C})$ stretching wavenumbers and the orientations of the vinyl groups, as induced by specific protein interactions, clearly showed that a lower frequency corresponds to a higher degree of conjugation between the C=C vinyl group and the porphyrin π system.⁴⁵ Increased conjugation from the vinyl groups shifts the energy not only of the $\pi \rightarrow \pi^*$ transition but also of the $a_{2u}(\pi) \rightarrow e_g(d_{\pi})$ (CT1) to lower energy, thus shifting the maxima to the red.^{32,45,46}

The RR spectra of Tf-trHb fluoride complexes are characterized by two overlapping $\nu(\text{C}=\text{C})$ bands at 1628 cm^{-1} , corresponding to vinyl groups with a low degree of conjugation with the heme. Mutations do not change the orientation of the vinyl group and, therefore, do not affect their conjugation, because the maximum frequency change of the $\nu(\text{C}=\text{C})$ stretches in the

Tf-trHb mutant series is 2 cm^{-1} (Table 1). Therefore, the observed changes of the CT1 maxima are solely due to different H-bonding interactions. In contrast, when the fluoride adducts of Mb, HRPC, and DHP are compared, the effect of the $\nu(\text{C}=\text{C})$ conjugation on the energy of the CT1 band must be taken into account. Mb-F is characterized by a higher degree of conjugation between the vinyl group and the porphyrin π system, as suggested by the presence of two overlapping $\nu(\text{C}=\text{C})$ at 1621 cm^{-1} .³² As a consequence, the CT1 band is at a lower energy compared to those of the Tf-trHb-F adducts. Less deviation from the line based on the Tf-trHb-F adducts is found for DHP, because a second weak vinyl mode is found at 1630 cm^{-1} .³⁹ Finally, the CT1 of the HRPC-F adduct is found at a energy higher than that of the Tf-trHb-F adducts. In fact, two vinyl stretches have been observed, as the band with a very low degree of conjugation between the vinyl group and the porphyrin π system (1631 cm^{-1}) is the most intense.³²

CONCLUSION

The present results can be considered as a unique data set, because they have been obtained for a complete group of mutants where the three key amino acids of Tf-trHb (WG8, YCD1, YB10) are progressively substituted with the non-hydrogen bonding phenylalanine. The spectroscopic characterization of the fluoride complexes has unveiled a well-defined correlation between $\nu(\text{Fe}-\text{F})$ vibrational frequencies and CT1 electronic transition energies. The validity of this correlation is confirmed by its being applicable to literature data, including important model proteins such as myoglobin and horseradish peroxidase. This indicates its general usefulness as an additional method to investigate relevant properties of the active site of heme proteins. For the case of Tf-trHb, we have obtained a detailed picture of H-bonding in the distal cavity environment. The interpretation of the spectroscopic data is strengthened by the close relation with the observed fluoride dissociation kinetics and molecular dynamics simulations. All the techniques yield evidence that TrpG8 and TyrCD1 can form strong H bonds with fluoride, whereas TyrB10 can only interact weakly.

ASSOCIATED CONTENT

S Supporting Information. Plot of rmsd vs time of MD simulation for the complexes between fluoride and WT Tf-trHb, YB10F, WG8F, YCD1F-WG8F, YB10F-YCD1F-WG8F mutants; time evolution of selected distances between distal residues of ASV Tf-trHb. The distances are defined as those between the coordinated fluoride and the following distal site atoms: indole N proton of the WG8, hydroxylic hydrogen of the YCD1, and the hydroxylic hydrogen of the YB10. Charges of selected atoms used in the simulation are given in Table S1. Kinetics of azide binding and release are given in Table S2. Azide release kinetics was calculated from the product of the measured thermodynamic and kinetic ligand binding data. This material is available free of charge via the Internet at <http://pubs.acs.org>.

AUTHOR INFORMATION

Corresponding Author
giulietta.smulevich@unifi.it

Author Contributions

[#]These authors contributed equally to this work.

ACKNOWLEDGMENT

This work was supported by Institute Pasteur Fondazione Cenci Bolognetti (A. Boffi), MIUR FIRB RBFRO8F41U_002 (A. Bonamore), MIUR PRIN 2008BFJ34 (A. Feis and A. Boffi), University of Buenos Aires (grant X074), CONICET, and European Union FP7 project NOSTress (D. Estrin), and the Italian Ministero dell'Istruzione, dell'Università e della Ricerca (MIUR), Direzione Generale per l'Internazionalizzazione della Ricerca, Progetti di Grande Rilevanza Italia-Argentina.

REFERENCES

- (1) Ma, L. H.; Liu, Y.; Zhang, X.; Yoshida, T.; La Mar, G. N. *J. Am. Chem. Soc.* **2006**, *128*, 6657–6668.
- (2) Streit, B. R.; Blanc, B.; Lukat-Rodgers, G. S.; Rodgers, K. R.; DuBois, J. L. *J. Am. Chem. Soc.* **2010**, *132*, 5711–5724.
- (3) Edwards, S. L.; Poulos, T. L. *J. Biol. Chem.* **1990**, *265*, 2588–2595.
- (4) Egawa, T.; Yeh, S. R. *J. Inorg. Biochem.* **2005**, *99* (1), 72–96.
- (5) Feis, A.; Lapini, A.; Catacchio, B.; Brogioni, S.; Foggi, P.; Chiancone, E.; Boffi, A.; Smulevich, G. *Biochemistry* **2008**, *47*, 902–910.
- (6) Ouellet, H.; Juszcak, L.; Dantsker, D.; Samuni, U.; Ouellet, Y. H.; Savard, P. Y.; Wittenberg, J. B.; Wittenberg, B. A.; Friedman, J. M.; Guertin, M. *Biochemistry* **2003**, *42*, 5764–5774.
- (7) Rodriguez, J. C.; Zeng, Y.; Wilks, A.; Rivera, M. *J. Am. Chem. Soc.* **2007**, *129*, 11730–11742.
- (8) Ye, X.; Demidov, A.; Rosca, F.; Wang, W.; Kumar, A.; Ionascu, D.; Zhu, L.; Barrick, D.; Wharton, D.; Champion, P. M. *J. Phys. Chem. A* **2003**, *107*, 8156–8165.
- (9) Springer, B. A.; Sligar, S. G.; Olson, J. S.; Phillips, G. N. *J. Chem. Rev.* **1994**, *94*, 699–714.
- (10) Quillin, M. L.; Li, T.; Olson, J. S.; Phillips, G. N., Jr.; Dou, Y.; Ikeda-Saito, M.; Regan, R.; Carlson, M.; Gibson, Q. H.; Li, H.; et al. *J. Mol. Biol.* **1995**, *245*, 416–436.
- (11) Wittenberg, J. B.; Bolognesi, M.; Wittenberg, B. A.; Guertin, M. *J. Biol. Chem.* **2002**, *277*, 871–874.
- (12) Bonamore, A.; Ilari, A.; Giangiacomo, L.; Bellelli, A.; Morea, V.; Boffi, A. *FEBS J.* **2005**, *272*, 4189–4201.
- (13) Nicoletti, F. P.; Comandini, A.; Bonamore, A.; Boechi, L.; Boubeta, F. M.; Feis, A.; Smulevich, G.; Boffi, A. *Biochemistry* **2010**, *49*, 2269–2278.
- (14) Droghetti, E.; Nicoletti, F. P.; Bonamore, A.; Boechi, L.; Arroyo Manez, P.; Estrin, D. A.; Boffi, A.; Smulevich, G.; Feis, A. *Biochemistry* **2010**, *49*, 10394–10402.
- (15) Droghetti, E.; Nicoletti, F. P.; Bonamore, A.; Sciamanna, N.; Boffi, A.; Feis, A.; Smulevich, G. *J. Inorg. Biochem.* **2011**, *105*, 1338–1343.
- (16) Jorgensen, W. L.; Chandrasekar, J.; Madura, J.; Impey, R. W.; Klein, M. L. *J. Chem. Phys.* **1983**, *79*, 926–935.
- (17) Luty, B. A.; Tironi, I. G.; Van Gunsteren, W. F. *J. Chem. Phys.* **1995**, *103*, 3014–3021.
- (18) Pearlman, D. A.; Case, D. A.; Caldwell, J. W.; Ross, W. S.; Cheatham, T. E.; Debolt, S.; Ferguson, D.; Seibel, G.; Kollman, P. *Comput. Phys. Commun.* **1995**, *91*, 1–41.
- (19) Boechi, L.; Manez, P. A.; Luque, F. J.; Marti, M. A.; Estrin, D. A. *Proteins* **2010**, *78*, 962–970.
- (20) Boechi, L.; Marti, M. A.; Milani, M.; Bolognesi, M.; Luque, F. J.; Estrin, D. A. *Proteins* **2008**, *73*, 372–379.
- (21) Crespo, A.; Marti, M. A.; Kalko, S. G.; Morreale, A.; Orozco, M.; Gelpi, J. L.; Luque, F. J.; Estrin, D. A. *J. Am. Chem. Soc.* **2005**, *127*, 4433–4444.
- (22) Marti, M. A.; Capece, L.; Bikiel, D. E.; Falcone, B.; Estrin, D. A. *Proteins* **2007**, *68*, 480–487.
- (23) Ye, L.; Spittler, D.; Ullrich, R.; Boland, W.; Nuske, J.; Diekert, G. *Biochemistry* **2010**, *49*, 7264–7271.
- (24) Asher, S. A.; Adams, M. L.; Schuster, T. M. *Biochemistry* **1981**, *20*, 3339–46.

- (25) Beetlestone, J.; George, P. *Biochemistry* **1964**, *3*, 707–714.
- (26) Tamura, M. *Biochim. Biophys. Acta* **1971**, *243*, 249–258.
- (27) Yonetani, T.; Wilson, D. F.; Seamonds, B. *J. Biol. Chem.* **1966**, *241*, 5347–5352.
- (28) Makinen, M. W.; Churg, A. K., in *Iron Porphyrins*, Lever, A.P.B. P; Gray, H.B. Eds, Addison-Wesley Publishing Company, Reading, USA, Part 1. 1983, 143–225.
- (29) Asher, S. A.; Vickery, L. E.; Schuster, T. M.; Sauer, K. *Biochemistry* **1977**, *16*, 5849–5856.
- (30) Desbois, A.; Lutz, M.; Banerjee, R. *Biochemistry* **1979**, *18*, 1510–1518.
- (31) Yu, N. T. *Methods Enzymol.* **1986**, *150*, 350–409.
- (32) Neri, F.; Kok, D.; Miller, M. A.; Smulevich, G. *Biochemistry* **1997**, *36*, 8947–8953.
- (33) Deatherage, J. F.; Loe, R. S.; Anderson, C. M.; Moffat, K. *J. Mol. Biol.* **1976**, *104*, 687–706.
- (34) Aime, S.; Fasano, M.; Paoletti, S.; Cutruzzola, F.; Desideri, A.; Bolognesi, M.; Rizzi, M.; Ascenzi, P. *Biophys. J.* **1996**, *70*, 482–488.
- (35) Coletta, M.; Ascoli, F.; Brunori, M.; Traylor, T. G. *J. Biol. Chem.* **1986**, *261*, 9811–9814.
- (36) Feis, A.; Santoni, E.; Neri, F.; Ciaccio, C.; De Sanctis, G.; Coletta, M.; Welinder, K. G.; Smulevich, G. *Biochemistry* **2002**, *41*, 13264–13273.
- (37) Belyea, J.; Belyea, C. M.; Lappi, S.; Franzen, S. *Biochemistry* **2006**, *45*, 14275–14284.
- (38) Feis, A.; Rodriguez-Lopez, J. N.; Thorneley, R. N.; Smulevich, G. *Biochemistry* **1998**, *37*, 13575–13581.
- (39) Nicoletti, F. P.; Thompson, M. K.; Howes, B. D.; Franzen, S.; Smulevich, G. *Biochemistry* **2010**, *49*, 1903–1912.
- (40) Smulevich, G.; Mantini, A. R.; Paoli, M.; Coletta, M.; Geraci, G. *Biochemistry* **1995**, *34*, 7507–7516.
- (41) Spiro, T. G.; Wasbotten, I. H. *J. Inorg. Biochem.* **2005**, *99*, 34–44.
- (42) Phillips, G. N., Jr.; Teodoro, M. L.; Li, T.; Smith, B.; Olson, J. S. *J. Phys. Chem. B* **1999**, *103*, 8817–8829.
- (43) Spiro, T. G.; Li, X.-Y. In *Biological application of Raman Spectroscopy*; Spiro, T. G., Ed.; Wiley Interscience: New York, 1988; Vol. 3, pp 1–37.
- (44) Kalsbeck, W. A.; A., G.; Pandey, R. K.; Smith, K. M.; Bocian, D. M. *J. Am. Chem. Soc.* **1995**, *117*, 10959–10968.
- (45) Marzocchi, M. P.; Smulevich, G. *J. Raman Spectrosc.* **2003**, *34*, 725–736.
- (46) Neri, F.; Indiani, C.; Baldi, B.; Vind, J.; Welinder, K. G.; Smulevich, G. *Biochemistry* **1999**, *38*, 7819–7827.
- (47) Sage, J. T.; Morikis, D.; Champion, P. M. *Biochemistry* **1991**, *30*, 1227–1237.